

Configurations of Nanocubes Floating and Clustering on Liquid Surfaces

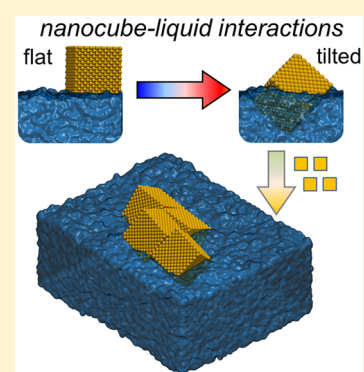
Tara A. Nitka,[†] Petr Král,[‡] and Lela Vuković^{*,†}

[†]Department of Chemistry and Biochemistry, University of Texas at El Paso, El Paso, Texas 79968, United States

[‡]Departments of Chemistry, Physics, and Biopharmaceutical Sciences, University of Illinois at Chicago, Chicago, Illinois 60607, United States

S Supporting Information

ABSTRACT: The configurations of nanoparticles (NPs) floating on liquid surfaces can be largely affected by the NP shapes in combination with different NP–liquid coupling strengths. Here, the behavior of ligated nanocubes (NCs) on liquid surfaces is studied as an example of such NP floating by analytical methods and molecular dynamics simulations. Depending on the NC–liquid coupling strength, NCs can sit on the liquid surface (weak), be partly immersed in a tilted orientation (intermediate), or be fully immersed except for the top facet (strong). The simulations reveal that configurations of clusters of self-assembled NCs on liquid surfaces can be even more complex and also determined by the NC–liquid and NC–NC coupling strengths, thus providing a rich spectrum of possible superstructures formed.



Advanced experimental techniques, established in the last two decades, have allowed the controlled synthesis of highly monodisperse colloidal nanoparticles (NPs) with a variety of compositions (cores and ligands),^{1,2} sizes,^{3–5} and shapes.^{6–11} Such high-quality NPs have been reproducibly self-assembled in bulk solutions,^{12,13} on various substrates,¹² and on the surfaces of solutions^{14–17} into many types of superstructures and superlattices. The resulting coarse materials have been of particular interest for their emergent sieving, optical, catalytic, magnetic, electronic, and thermo-electric properties.^{19–25}

Recent studies have revealed that spherical NPs can self-assemble on liquid surfaces into ultrathin single or binary superlattices (SLs or BNSLs). The submergence depth of NPs on liquid surfaces is controlled by the surface energies of the liquids and the strengths of NP–liquid coupling,¹⁶ where the types of superstructures formed are determined by a delicate balance of anisotropic (surface) forces of comparable magnitudes acting in these systems.^{16,26} These forces originate in van der Waals (vdW), Coulombic, hydrophobic, and other types of coupling¹ given by the types of NPs, solvents, external fields, and substrates used.

The self-assembly of aspherical NPs on liquid surfaces can be particularly complex and lead to a rich spectrum of superstructures. Here, we use analytical modeling and molecular dynamics simulations to study nanocubes (NCs) floating on liquid surfaces and examine the initial stages of their clustering. In order to rationally design and synthesize NPs superlattices at liquid surfaces, it is crucial to understand the NPs' self-assembly mechanisms through a detailed modeling.

Recent experimental and molecular dynamics (MD) studies revealed that spherical NPs floating on liquid surfaces favor semi-immersed positions.¹⁶ However, it is less obvious how *aspherical* NPs float on liquid surfaces and self-assemble, dependent on the NP–liquid coupling strengths. Here, we address these problems first by performing analytical modeling to estimate the free energy of NC–liquid binding, ΔG , as a function of an NC orientation and an immersion height, h . Then, atomistic modeling is performed for naked and ligated NCs at the water surface, considering a variable NC–liquid coupling strength. Finally, the clustering of several NCs on liquid surfaces is simulated.

Analytical Modeling of NCs Floating on Liquid Surfaces. Here, we examine the floating modes of NCs on liquid surfaces, using a simple analytical model for calculating Gibbs free energies of individual NCs immersed in liquids, by expanding a previously established basic procedure.¹⁶

As the NC becomes immersed in the liquid, it creates an excess surface of the liquid due to the formation of a cavity in it. The Gibbs free energy cost, G_1 , to create the excess liquid surface area, A_{excess} , can be estimated as $G_1 = \gamma A_{\text{excess}}$, where γ is the surface tension of the liquid. G_1 is offset by favorable (mostly dispersive) interactions between molecules. These interactions can be evaluated from the free energy, $G_2 = G^\circ A_{\text{immerse}}$, where G° is the free energy of NC–liquid binding per unit area and A_{immerse} is the immersed surface area of the NC. To gain a better idea about G_1 and G_2 , a model system is

Received: June 6, 2019

Accepted: June 11, 2019

Published: June 11, 2019

built with parameters evaluated for NC with a dodecanethiol-passivated metal core, floating on diethylene glycol (DEG). Then, we used $G^\circ \approx -7$ kcal/(mol·nm²) and $\gamma \approx 45$ dyn/cm, as in our earlier related studies.¹⁶

Figure 1A shows that the NC immersion in the liquid could occur in flat and tilted orientations. Considering an NC with

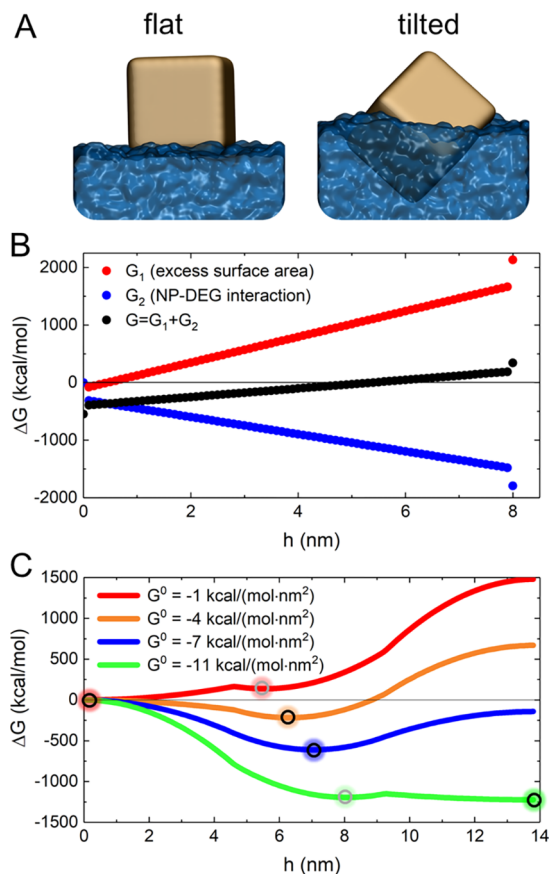


Figure 1. Analytical model of NCs submerged at liquid surfaces. (A) Schematic of NCs in flat and tilted orientations submerged in liquid. (B) Free energy of an NC–DEG coupling, ΔG , as a function of immersion height, h , for a flat NC orientation. The considered NC has a 5 nm solid core, protected with a 1.5 nm thick ligand shell (alkane), and is floating on diethylene glycol (DEG) (Methods).¹⁶ (C) Total free energy of NC–DEG coupling, ΔG , as a function of NC immersion (tilted, body diagonal is vertical) height, h . The NC size is as in panel B, but the strengths of favorable interactions between ligands and DEG per unit of contact area are varied according to the values of G° given in the legend. The black and gray circles mark the global and local minima in ΔG , respectively.

the above parameters and the flat orientation, Figure 1B shows the G_1 , G_2 , and $\Delta G = G_1 + G_2$ dependences on the NC immersion height h . They are obtained from $G_1 \propto k_1 h$ and $G_2 \propto G_{\text{facet}} - k_2 h$ ($k_{1,2} > 0$), where $G_{\text{facet}} < 0$ is a free energy of binding of a single (bottom) NC facet to DEG and k_1 and k_2 parameters depend on γ and G° . For the present γ and G° , G_1 dominates ($k_1 > k_2$), giving $\Delta G \propto G_{\text{facet}} + (k_1 - k_2)h$ with an absolute minimum of $\Delta G = G_{\text{facet}}$ at $h = 0$ and a linear growth for $h > 0$ (except at h , where G_1 , G_2 , and ΔG change discontinuously once the top NC facet submerges). Therefore, the selected NC should be lying flat on top of DEG. When the NC–liquid coupling, G° , is increased by changing the ligands or the underlying liquid, G_2 should eventually surpass G_1 ($k_2 >$

k_1) and NCs should gradually submerge in DEG. Because we consider so far only the flat NC orientation, ΔG would have a negative slope and reach an absolute minimum when NC is fully immersed, except the top facet. Therefore, because of the linear dependence of ΔG on h , NCs in a flat orientation can either sit on the top of the liquid (weak NC–liquid coupling) or be fully immersed in it (strong NC–liquid coupling). In contrast, in spherical NPs, $G_1 \propto k_1' h^2$ and $G_2 \propto -k_2' h$, giving a local minimum in ΔG at certain h .¹⁶

Next, we separately explore NCs in tilted configurations, having, for simplicity, a body diagonal orthogonal to the liquid surface, as shown in Figure 1A. Figure 1C gives ΔG in such cases as a function of h and parameters as before, except the varied NC coupling to DEG interface (G°). Notice that when G° is too small or too large, ΔG predicts that NC is either fully exposed (weak coupling, e.g. $G^\circ \geq -1$ kcal/(mol·nm²)) or fully submerged (strong coupling, e.g. $G^\circ \leq -11$ kcal/(mol·nm²)). However, for intermediate NC–liquid coupling strengths (-4 kcal/(mol·nm²) $\leq G^\circ \leq -7$ kcal/(mol·nm²)), minima in ΔG are observed to form for partly (approximately half) immersed NCs. In these intermediate cases, we need to assume that NCs are tilted and partly submerged in liquid, as in spherical NPs.

MD Simulations of NCs Floating on Liquid Surfaces. To understand better the nature of NC immersion regimes predicted by the analytical model, next, MD simulations of naked solid NCs (fcc gold, 3 nm edge length) at the water surface were carried out. For simplicity, different NC–water coupling strengths were modeled by varying a parameter ϵ of the vdW coupling strength in all NC atoms (Methods). Water was selected because of its low viscosity (in contrast to DEG), so that NCs can quickly equilibrate on the MD simulation time scale.

Panels A and B of Figure 2 show the equilibrated configurations of NCs at the water surface. For low NC–water coupling strengths ($\epsilon > -0.1$ kcal/mol), NCs remained on the water surface without immersing, whereas for strong NC–water coupling strengths ($\epsilon < -0.5$ kcal/mol), NCs immersed into water. At intermediate NC–water coupling strengths (-0.45 kcal/mol $< \epsilon < -0.1$ kcal/mol), NCs were partly submerged in tilted orientations.

Figure 2C shows the contact areas between NCs and water as a function of ϵ . The NC–water contact area increases from ~ 3800 Å² ($\epsilon = -0.2$ kcal/mol) to ~ 6800 Å² ($\epsilon = -0.45$ kcal/mol), showing that NCs with a stronger coupling to water become gradually submerged, like spherical NPs.¹⁶ Interestingly, body diagonals of NCs in tilted orientations are misaligned by several degrees from the vector normal to the liquid surface (4.5° – 6.7°), as shown in Figure 2D.

Panels E–G of Figure 2, obtained also by MD simulations, reveal how NCs coated with organic ligands of different hydrophobicity float and submerge in water. The NCs had hydrophobic (alkane, $-\text{S}(\text{CH}_2)_{11}\text{CH}_3$), moderately hydrophobic (ether-terminated, $-\text{S}(\text{CH}_2)_{11}\text{OCH}_3$), or hydrophilic (alcohol-terminated, $-\text{S}(\text{CH}_2)_{12}\text{OH}$) ligands. Upon their equilibration in MD simulations, NCs with alkane ligands do not immerse, NCs with ether-terminated ligands assume tilted orientations, and NCs with alcohol-terminated ligands immerse in water. Ligands present on hydrophilic NC can part at edges, leaving the hydrophobic alkyl groups of the ligand exposed, resulting in incomplete NC immersion (Figure 2G; ligand parting is shown more clearly in Figure S3). As ligand parting leads to creation of significant hydrophobic

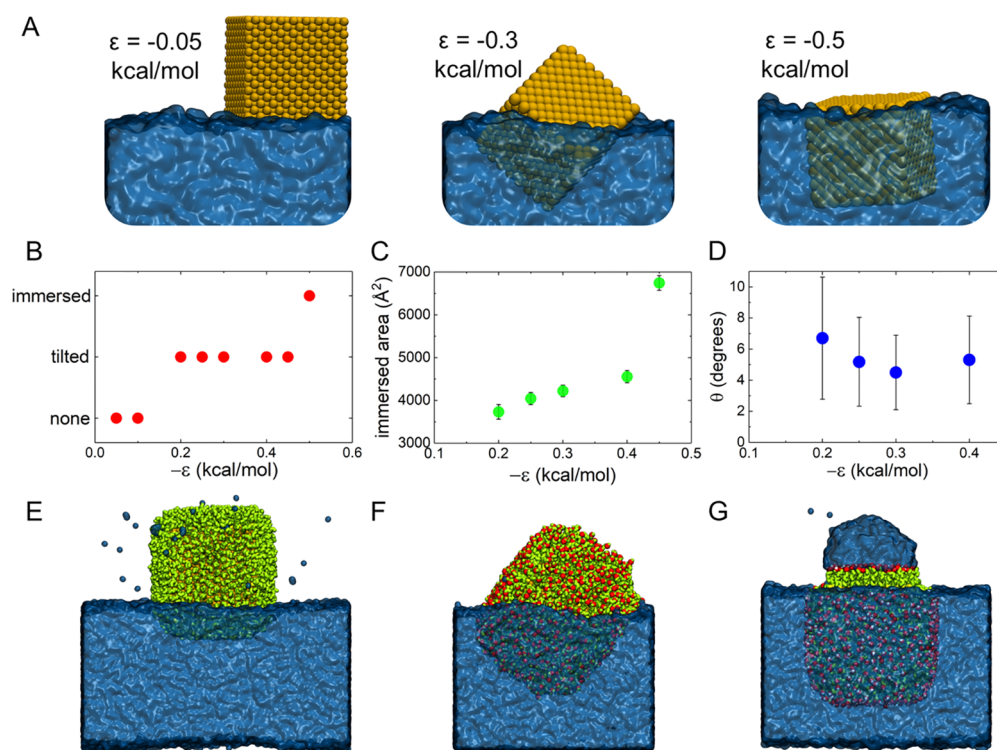


Figure 2. (A) Three solvation regimes of NCs at the water surface, dependent on the vdW parameter, ϵ , of all NC atoms, as obtained in MD simulations. (B) NC immersion regimes as a function of ϵ : no immersion, tilted immersion, and full immersion. (C) The immersed surface areas of NCs as a function of ϵ . (D) Average angle, θ , that NC body diagonal forms with the normal vector of the liquid interface, shown for NCs in tilted immersed states. Data shown in panels C and D are averaged over the last 90 ns of trajectories. (E–G) Three solvation regimes of ligated NCs equilibrated for 100 ns at the water surface: NC coated with (E) $-\text{S}(\text{CH}_2)_{11}\text{CH}_3$ ligands, (F) $-\text{S}(\text{CH}_2)_{11}\text{OCH}_3$ ligands, and (G) $-\text{S}(\text{CH}_2)_{12}\text{OH}$ ligands.

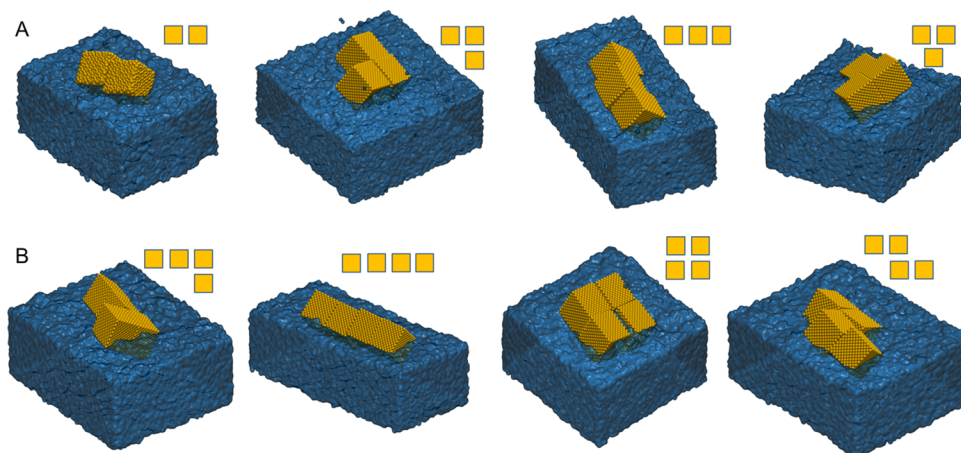


Figure 3. (A) Configurations of two or three NC clusters ($\epsilon = -0.3$ kcal/mol) in different initial arrangements (insets). In the initial states, the NCs have 45 or 50 Å center-to-center distances. (B) Configurations of four NC clusters ($\epsilon = -0.3$ kcal/mol) in different initial arrangements (insets). In the initial state, the NCs have 45 Å center-to-center distances. All the snapshots are obtained after 100 ns of equilibration.

surfaces that water avoids, a water droplet is formed on the NC top, which is hydrophilic because of the terminal $-\text{OH}$ groups of the ligands.

MD Simulations of NC Clustering. Finally, we tested the clustering of 2–4 naked NCs ($\epsilon = -0.3$ kcal/mol) on water. Initially, these NCs were slightly separated and half-immersed in water in flat orientations in (linear, L-shaped, staggered, or shifted) arrangements shown in Figure 3 (insets). While many other NC arrangements can be formed in experiments, these representative arrangements are selected to exemplify the

structural richness of possible self-assembled structures. Once the systems started to be simulated, NCs quickly tilted from the initial flat orientations, approached each other via diffusion, and bound via neighboring facets, thus forming stable aggregates, as shown in Figures 3 and S1 (equilibration for 100 ns). Although the NCs' binding was robust, individual NCs were not perfectly aligned. Instead, they had slightly shifted facet-to-facet contacts (Figure 3A, middle) or they were rotated with respect to each other (Figure 3B, right). Interestingly, small aggregates of NCs favored tilted immersed

configurations, similar to individual NCs, where the aggregate shapes determined different immersions of individual NCs. One can expect that similar configurations can be obtained for NCs fully exposed or fully submerged in liquids, although without being tilted. These NC organization principles also determine the self-assembly of larger superlattices, which would be possible to examine with coarse-grained simulations. When more NCs are present on the liquid–air interface, two-dimensional superlattices with periodically arranged NCs are expected to form, where the orientation of NCs should depend on the NC–liquid coupling strength and other parameters. For example, one could imagine the formation of “Janus-type” superstructures from hybrid types of NCs, where one type would be submerged and the other type attached to it and floating above it.

In conclusion, we have examined the immersion and clustering (limited self-assembly) of anisotropic NCs at liquid surfaces, using analytical modeling and atomistic MD simulations. It was revealed that the strength of NC–liquid interactions influences the immersion and orientations of NCs and their aggregates. NCs at liquid surfaces had three different and distinct immersion regimes, being in flat orientation on top of the liquid, approximately half-immersed in a tilted orientation, or fully immersed, as NC–liquid coupling increases, in contrast to spherical NPs,¹⁶ which became gradually more immersed as NP–liquid coupling increased. While our solid core NCs had perfect cubic shapes, the ligated NCs had rounded corners. Despite this difference, these NCs show the same immersion behavior as perfect NCs. However, if NCs had further cut corners, their immersion behavior would eventually become similar to the behavior of spherical NPs, so the NP would gradually immerse into the liquid as NP–liquid coupling increases (distinct immersion regimes would disappear). The submersion and floating of different types of NPs, such as tetrahedral NPs, rods, etc. could lead to the formation of many atypical superstructures. Experiments, such as those conducted in ref 18, could be used to examine in situ self-assembly of NCs and other anisotropic NPs on liquid surfaces. The knowledge of NPs’ behavior at liquid surfaces could be implemented in designs of NP-based materials.

METHODS

To understand the immersion behavior of single NCs at liquid surfaces, we examined the major energetic contributions to NC solvation.

Analytical Model. When a dodecanethiol-passivated metal NC immerses in DEG,¹⁶ it creates a cavity with excess liquid surface area, A_{excess} . The Gibbs free energy cost to create the excess surface area is $G_1 = \gamma A_{\text{excess}} = \gamma(A_{\text{immerse}} - A_{\text{slice}})$, where γ is the surface tension of DEG (≈ 45 dyn/cm), A_{immerse} the immersed surface area of NC, and A_{slice} the surface area of the liquid prior to NC immersion. A_{immerse} and A_{slice} depend on the NC orientation at the interface. For a flat NC orientation at the liquid surface (Figure 1A)

$$A_{\text{immerse}} = \begin{cases} a^2 + 4h^2, & h < a \\ 2a^2 + 4h^2, & h = a \end{cases} \quad (1)$$

and

$$A_{\text{slice}} = a^2 \quad (2)$$

where a is the length of the NC edge and h is the NC immersion height.

For NCs in the tilted orientation (Figures 1A and S2)

$$A_{\text{immerse}} = \begin{cases} \frac{9}{2}h^2, & h \leq h_1 \\ \frac{9}{2}h_1^2 + \frac{3\sqrt{2}}{2}a(h - h_1), & h_1 < h \leq h_2 \\ \frac{9}{2}h_1^2 + \frac{\sqrt{6}}{2}a^2 + \frac{9}{2}(h_1^2 - (h - h_3)^2), & h > h_2 \end{cases} \quad (3)$$

where $h_1 = \frac{\sqrt{3}}{3}a$, $h_2 = \frac{2\sqrt{3}}{3}a$, and $h_3 = \sqrt{3}a$ and

$$A_{\text{slice}} = \begin{cases} \frac{3\sqrt{3}}{2}h^2, & h \leq h_1 \\ \frac{3\sqrt{3}}{2}h^2 - \frac{9\sqrt{3}}{2}(h - h_1)^2, & h_1 < h \leq h_2 \\ \frac{3\sqrt{3}}{2}(h_3 - h)^2, & h > h_2 \end{cases} \quad (4)$$

The Gibbs free energy cost of creating excess liquid surface area is offset by favorable interactions between the liquid and the NC surface. These favorable interactions are evaluated as $G_2 = G^\circ A_{\text{immerse}}$, where G° is the free energy of NC–liquid binding per unit area. For the dodecanethiol-passivated gold NP immersed in DEG, $G^\circ \approx -7$ kcal/mol·nm².¹⁶ A wider range of G° is probed in modeling the immersion of NCs in tilted orientations, as defined in the legend of Figure 1C. Therefore, we scan different NC–liquid binding strengths to ensure the validity of our model for different types of NCs and liquids. The total Gibbs free energy of NC–liquid binding as a function of immersion height is obtained as $\Delta G = G_1 + G_2$. This model neglects the effects of gravity, because the gravitational potential energy of an NC (7.9×10^{-10} kcal/mol for 3.07 nm edge gold NC to move by 1 nm because of gravity) is orders of magnitude smaller than the NC–liquid interaction energy (several kilocalories per mole per 1 nm² surface of NC).

Molecular Dynamics Simulations. Atomistic simulations were performed to investigate the behavior of NCs on liquid surfaces. In all simulations, solid core NCs were prepared by cutting a face-centered cubic lattice, based on gold atoms (Au–Au bond length of 2.88 Å), into NCs with 3.07 nm (naked) or 5.1 nm (ligated) edge lengths. In systems where ligand-coated NCs were studied, thiolated ligands were covalently bound via Au–S bonds to NC facets, with the surface density of 0.3949 ligands per one Au atom. Three types of ligands were examined: $-\text{S}(\text{CH}_2)_{11}\text{CH}_3$, $-\text{S}(\text{CH}_2)_{11}\text{OCH}_3$, and $-\text{S}(\text{CH}_2)_{12}\text{OH}$. These ligands were built in the Gaussview graphical interface and distributed on NC facets using our own code. The prepared solid core and ligated NCs were solvated in TIP3P water with the *solvate* VMD plugin.²⁷ In simulations, NCs were initially positioned halfway immersed at the water surface.

Atoms of solid core NCs had varying vdW coupling parameter, ϵ , which controls the strength of NC–water interactions. In our simulations, $\epsilon = -0.1, -0.2, -0.25, -0.3, -0.4, -0.45, -0.5$, and -0.7 kcal/mol were selected as model coupling strengths. In systems with ligated NCs, the ligands were described with CHARMM36 general force field

parameters.^{28,29} MD simulations were performed with the NAMD2.12 package.³⁰ All simulations were conducted with Langevin dynamics (a Langevin constant of $\gamma_{\text{Lang}} = 0.01 \text{ ps}^{-1}$) in the NVT ensemble at $T = 300 \text{ K}$. The particle-mesh Ewald method was used to calculate long-range Coulomb interaction energies, with periodic boundary conditions applied in all directions.³¹ The time step was set to 2.0 fs. The evaluation of long-range vdW and Coulombic interactions was performed every 1 and 2 time steps, respectively. After 20 000 steps of minimization, the systems were equilibrated. All the systems examined and the simulations performed are summarized in Table S1. Images of simulated systems were prepared using VMD and Tachyon ray tracing.²⁷

Data Analysis. The extent of immersion of solid core NCs at the water surface was characterized by calculating the NC–water surface area, $a_{\text{imm}}(t)$, as a function of time, defined as

$$a_{\text{imm}}(t) = \frac{1}{2}(a_{\text{NC}} + a_{\text{sol}}(t) - a_{\text{tot}}(t)) \quad (5)$$

where a_{NC} , $a_{\text{wat}}(t)$, and $a_{\text{tot}}(t)$ are the solvent accessible surface areas (SASAs) of the NC, water, and NC and water together, respectively. The evaluation was done by the SASA built-in VMD plugin.²⁷

For solid core NCs in tilted orientations, average angles between their body diagonals and the vector normal to the liquid surface were calculated. Each body diagonal was taken to be the vector from a Au atom on one corner of the cube (either the most deeply immersed or opposite of the most deeply immersed corner) and the center of the 3 Au atoms at the opposite corner of the cube.

■ ASSOCIATED CONTENT

Supporting Information

The Supporting Information is available free of charge on the ACS Publications website at DOI: 10.1021/acs.jpcl.9b01638.

Table with simulation details, images of additional systems of self-assembled NCs, and plots of areas derived in eqs 3 and 4 (PDF)

■ AUTHOR INFORMATION

Corresponding Author

*E-mail: lvukovic@utep.edu.

ORCID

Tara A. Nitka: 0000-0001-9435-6515

Petr Král: 0000-0003-2992-9027

Lela Vuković: 0000-0002-9053-5708

Notes

The authors declare no competing financial interest.

■ ACKNOWLEDGMENTS

The authors gratefully acknowledge the computer time provided by the Texas Advanced Computing Center (TACC).

■ REFERENCES

- (1) Bishop, K. J. M.; Wilmer, C. E.; Soh, S.; Grzybowski, B. A. Nanoscale Forces and Their Uses in Self-Assembly. *Small* **2009**, *5*, 1600–1630.
- (2) Albanese, A.; Tang, P. S.; Chan, W. C. W. The Effect of Nanoparticle Size, Shape, and Surface Chemistry on Biological Systems. *Annu. Rev. Biomed. Eng.* **2012**, *14*, 1–16.

- (3) Hussain, I.; Graham, S.; Wang, Z.; Tan, B.; Sherrington, D. C.; Rannard, S. P.; Cooper, A. I.; Brust, M. Size-Controlled Synthesis of Near-Monodisperse Gold Nanoparticles in the 1–4 nm Range Using Polymeric Stabilizers. *J. Am. Chem. Soc.* **2005**, *127*, 16398–16399.

- (4) Mohamed, M. B.; Wang, Z. L.; El-Sayed, M. A. Temperature-Dependent Size-Controlled Nucleation and Growth of Gold Nanoclusters. *J. Phys. Chem. A* **1999**, *103*, 10255–10259.

- (5) Wang, J.; Neoh, K. G.; Kang, E. T. Preparation of Nanosized Metallic Particles in Polyaniline. *J. Colloid Interface Sci.* **2001**, *239*, 78–86.

- (6) Yin, Y.; Alivisatos, A. P. Colloidal Nanocrystal Synthesis and the Organic-Inorganic Interface. *Nature* **2005**, *437*, 664–670.

- (7) Min, Y.; Akbulut, M.; Kristiansen, K.; Golan, Y.; Israelachvili, J. The Role of Interparticle and External Forces in Nanoparticle Assembly. *Nat. Mater.* **2008**, *7*, 527.

- (8) Tao, A. R.; Habas, S.; Yang, P. Shape Control of Colloidal Metal Nanocrystals. *Small* **2008**, *4*, 310–325.

- (9) Srivastava, S.; Kotov, N. A. Nanoparticle Assembly for 1D and 2D Ordered Structures. *Soft Matter* **2009**, *5*, 1146–1156.

- (10) Chan, H.; Demortière, A.; Vuković, L.; Král, P.; Petit, C. Colloidal Nanocube Supercrystals Stabilized by Multipolar Coulombic Coupling. *ACS Nano* **2012**, *6*, 4203–4213.

- (11) Tan, S. F.; Raj, S.; Bisht, G.; Annadata, H. V.; Nijhuis, C. A.; Král, P.; Mirsaidov, U. Nanoparticle Interactions Guided by Shape-Dependent Hydrophobic Forces. *Adv. Mater.* **2018**, *30*, 1707077.

- (12) Shevchenko, E. V.; Talapin, D. V.; Kotov, N. A.; O'Brien, S.; Murray, C. B. Structural Diversity in Binary Nanoparticle Superlattices. *Nature* **2006**, *439*, 55–59.

- (13) Talapin, D. V.; Shevchenko, E. V.; Bodnarchuk, M. I.; Ye, X.; Chen, J.; Murray, C. B. Quasicrystalline Order in Self-Assembled Binary Nanoparticle Superlattices. *Nature* **2009**, *461*, 964.

- (14) Dong, A.; Chen, J.; Vora, P. M.; Kikkawa, J. M.; Murray, C. B. *Nature* **2010**, *466*, 474.

- (15) Singh, G.; Chan, H.; Baskin, A.; Gelman, E.; Repnin, N.; Král, P.; Klajn, R. Self-Assembly of Magnetite Nanocubes into Helical Superstructures. *Science* **2014**, *345*, 1149.

- (16) Udayabhaskararao, T.; Altantzis, T.; Houben, L.; Coronado-Puchau, M.; Langer, J.; Popovitz-Biro, R.; Liz-Marzán, L. M.; Vuković, L.; Král, P.; Bals, S.; Klajn, R. Tunable Porous Nanoalloy Structures Prepared by Post-Assembly Etching of Binary Nanoparticle Superlattices. *Science* **2017**, *358*, 514.

- (17) Kim, D.; Bae, W. K.; Kim, S.-H.; Lee, D. C. Depletion-Mediated Interfacial Assembly of Semiconductor Nanorods. *Nano Lett.* **2019**, *19*, 963–970.

- (18) Miele, E.; Raj, S.; Baraissov, Z.; Král, P.; Mirsaidov, U. Dynamics of Templated Assembly of Nanoparticle Filaments within Nanochannels. *Adv. Mater.* **2017**, *29*, 1702682.

- (19) Shevchenko, E. V.; Ringler, M.; Schwemer, A.; Talapin, D. V.; Klar, T. A.; Rogach, A. L.; Feldmann, J.; Alivisatos, A. P. Self-Assembled Binary Superlattices of CdSe and Au Nanocrystals and Their Fluorescence Properties. *J. Am. Chem. Soc.* **2008**, *130*, 3274–3275.

- (20) Kang, Y.; Ye, X.; Chen, J.; Cai, Y.; Diaz, R. E.; Adzic, R. R.; Stach, E. A.; Murray, C. B. Design of Pt-Pd Binary Superlattices Exploiting Shape Effects and Synergistic Effects for Oxygen Reduction Reactions. *J. Am. Chem. Soc.* **2013**, *135*, 42–45.

- (21) Yang, Y.; Wang, B.; Shen, X.; Yao, L.; Wang, L.; Chen, X.; Xie, S.; Li, T.; Hu, J.; Yang, D.; Dong, A. Scalable Assembly of Crystalline Binary Nanocrystal Superparticles and Their Enhanced Magnetic and Electrochemical Properties. *J. Am. Chem. Soc.* **2018**, *140*, 15038–15047.

- (22) Chen, J.; Dong, A.; Cai, J.; Ye, X.; Kang, Y.; Kikkawa, J. M.; Murray, C. B. Collective Dipolar Interactions in Self-Assembled Magnetic Binary Nanocrystal Superlattice Membranes. *Nano Lett.* **2010**, *10*, 5103–5108.

- (23) Urban, J. J.; Talapin, D. V.; Shevchenko, E. V.; Kagan, C. R.; Murray, C. B. Synergism in Binary Nanocrystal Superlattices Leads to Enhanced p-type Conductivity in Self-Assembled PbTe/Ag₂Te Thin Films. *Nat. Mater.* **2007**, *6*, 115.

(24) Cargnello, M.; Johnston-Peck, A. C.; Diroll, B. T.; Wong, E.; Datta, B.; Damodhar, D.; Doan-Nguyen, V. V. T.; Herzing, A. A.; Kagan, C. R.; Murray, C. B. Substitutional Doping in Nanocrystal Superlattices. *Nature* **2015**, *524*, 450.

(25) Ibanez, M.; Luo, Z.; Genç, A.; Piveteau, L.; Ortega, S.; Cadavid, D.; Dobrozhan, O.; Liu, Y.; Nachtegaal, M.; Zebarjadi, M.; Arbiol, J.; Kovalenko, M. V.; Cabot, A. High-Performance Thermoelectric Nanocomposites from Nanocrystal Building Blocks. *Nat. Commun.* **2016**, *7*, 10766.

(26) Vuković, L.; Král, P. Coulombically Driven Rolling of Nanorods on Water. *Phys. Rev. Lett.* **2009**, *103*, 246103.

(27) Humphrey, W.; Dalke, A.; Schulten, K. VMD: Visual Molecular Dynamics. *J. Mol. Graphics* **1996**, *14*, 33–38.

(28) Vanommeslaeghe, K.; Hatcher, E.; Acharya, C.; Kundu, S.; Zhong, S.; Shim, J.; Darian, E.; Guvench, O.; Lopes, P.; Vorobyov, I.; Mackerell, A. D., Jr. CHARMM General Force Field: A Force Field for Drug-Like Molecules Compatible with the CHARMM All-Atom Additive Biological Force Fields. *J. Comput. Chem.* **2009**, *31*, 671–690.

(29) Yu, W.; He, X.; Vanommeslaeghe, K.; MacKerell, A. D., Jr. Extension of the CHARMM General Force Field to Sulfonyl-Containing Compounds and Its Utility in Biomolecular Simulations. *J. Comput. Chem.* **2012**, *33*, 2451–2468.

(30) Phillips, J. C.; Braun, R.; Wang, W.; Gumbart, J.; Tajkhorshid, E.; Villa, E.; Chipot, C.; Skeel, R. D.; Kalé, L.; Schulten, K. Scalable Molecular Dynamics with NAMD. *J. Comput. Chem.* **2005**, *26*, 1781–1802.

(31) Darden, T.; York, D.; Pedersen, L. Particle Mesh Ewald: An $N \cdot \log(N)$ Method for Ewald Sums in Large Systems. *J. Chem. Phys.* **1993**, *98*, 10089–10092.